Mechanical Failure of Fresh Nuclear Grade Iron-Chromium-Aluminum (FeCrAl) Cladding Under Simulated Hot Zero Power Reactivity Initiated Accident Conditions[†]

Nicholas R. Brown[1,*], Benton E. Garrison[2,*], Richard R. Lowden[2], M. Nedim Cinbiz[2,3], Kory D. Linton[2]

[1] University of Tennessee-Knoxville, Knoxville, TN 37913
[2] Oak Ridge National Laboratory, Oak Ridge, TN 37830
[3] Present affiliation: Idaho National Laboratory, Idaho Falls, ID 83402

* The authors N. R. Brown and B. E. Garrison are considered co-first authors and equal contributors to this manuscript. Corresponding author: nbrown49@utk.edu (N. R. Brown)

Abstract

The reactivity initiated accident (RIA) is a postulated accident in light water reactors initiated by a rapid increase in reactivity which causes an increase in fission rate and fuel temperature. One potential mode of fuel system failure during RIA is pellet cladding mechanical interaction (PCMI) due to the rapid thermal expansion of the fuel pellet. Simulated PCMI experiments were performed by rapidly pressurizing cladding tube samples using a hydraulic modified burst test system, causing the specimens to burst under a biaxial loading path. Deformation and rupture of the specimens were tracked with a telecentric lens and high-speed camera system. Outer surface strains were calculated using digital image correlation (DIC) on speckle patterns painted on the specimens' outer surfaces. Experiments were conducted at approximately 275°C, representative of hot zero power RIA conditions. The failure hoop strain was DIC-calculated between approximately 1.8–3.4%, corresponding to quasi-static energy depositions of approximately 110–260 calories per gram UO_2 assuming initial pellet-cladding contact. These conditions are very similar to the proposed energy deposition limit of 150 calories per gram UO_2 for unirradiated zirconium-based cladding in US Nuclear Regulatory Commission (NRC) Draft Regulatory Guide 1327. A very small strain rate dependence was observed in the data, with the magnitude of the failure hoop strain decreasing slightly with increasing strain rate. This observed dependence may be relevant because the iron-chromium-aluminum (FeCrAl) cladding strain rate will be approximately 20% higher than in zirconium-based cladding due to the harder neutron spectrum and resultant shorter neutron generation time.

1. Introduction

Nuclear-grade iron-chromium-aluminum (FeCrAl) cladding alloy C26M, a leading candidate for *IronClad*™ [1], has been established as a leading candidate accident-tolerant fuel (ATF) cladding material [2]. FeCrAl cladding is currently being irradiated as lead test rods (LTRs) in the Hatch

---

[†] This manuscript has been co-authored by UT-Battelle, LLC, under contract DE-AC05-00OR22725 with the US Department of Energy (DOE). The US government retains and the publisher, by accepting the article for publication, acknowledges that the US government retains a nonexclusive, paid-up, irrevocable, worldwide license to publish or reproduce the published form of this manuscript, or allow others to do so, for US government purposes. DOE will provide public access to these results of federally sponsored research in accordance with the DOE Public Access Plan (http://energy.gov/downloads/doe-public-access-plan).

Boiling Water Reactor (BWR). The objective of ATF cladding such as FeCrAl is to preserve or improve the current performance and safety characteristics of light-water reactors (LWRs). This includes during a postulated reactivity-initiated accident (RIA) [3]. The primary initiating event considered for RIA is a control rod ejection in a pressurized water reactor (PWR) or a control rod drop in a BWR. This paper presents the results of separate effects tests that were conducted to provide data relevant to establishing safety limits for FeCrAl cladding in postulated RIA events in LWRs. The separate effects test data is also functional for establishing conditions for integral reactivity-initiated accident (RIA) testing in the TREAT reactor at Idaho National Laboratory (INL).

An RIA causes a prompt increase of the fission-rate density in nuclear fuel. Most of the energy associated with the fission-rate density is promptly deposited in the fuel (approximately 90%) [4]. The deposited energy causes the fuel temperature to rapidly increase, and the fuel experiences thermal expansion. During fuel thermal expansion, if the fuel-cladding gap is already closed or closes during RIA, the expansion of fuel induces mechanical strain on the cladding. This is known as the pellet-cladding mechanical interaction (PCMI) phase of the RIA. In a super prompt RIA, the events can occur with pulse widths as short as tens of milliseconds (see Figure 1). The event is terminated by prompt inherent feedback (i.e., the Doppler coefficient in an LWR). If the mechanical strain on the cladding is sufficient, the cladding may rupture. US Nuclear Regulatory Commission (NRC) Draft Regulatory Guide 1327 (DG-1327) presents energy deposition limits expressed as total peak radial average fuel enthalpy increase in calories per gram UO_2 for zirconium-based cladding [5]. These limits indicate that cladding failure is expected at 150 calories per gram UO_2 for several types of fresh zirconium-based cladding.

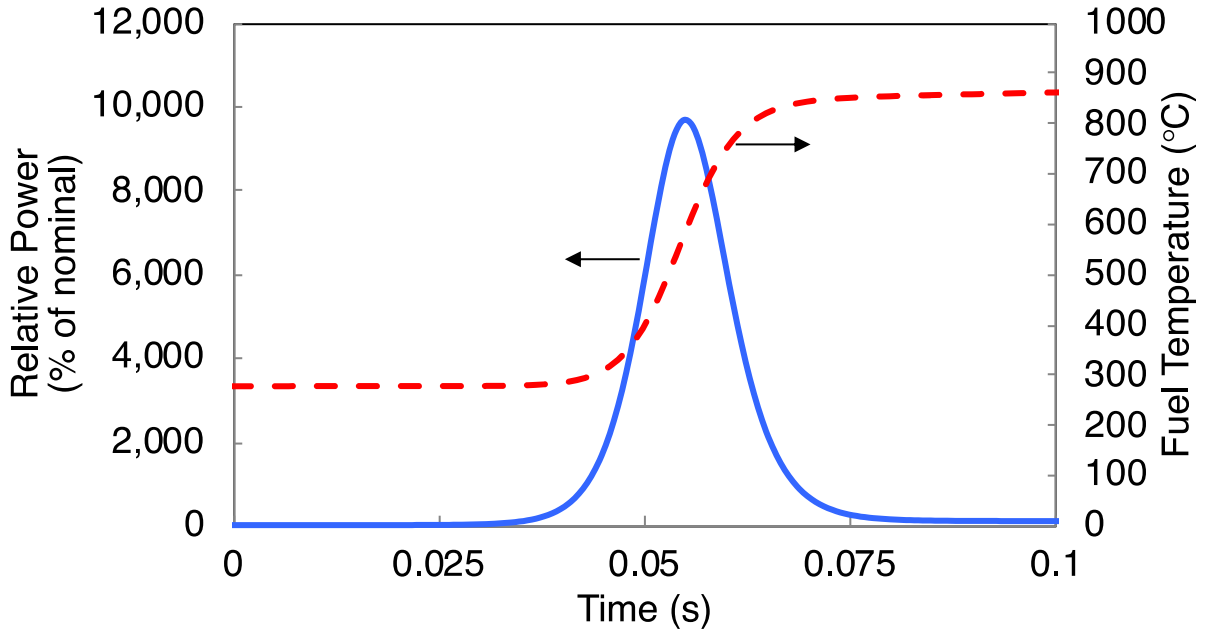

Figure 1. Example RIA showing the prompt increase in fission rate that is terminated by the prompt inherent feedback.

RIA imposes special mechanical loading conditions on the cladding tubes. Under RIA PCMI, cladding tubes are expected to be under a multiaxial and strain-driven loading condition with strain rates of 1–5 s^{-1} [6]. This paper is focused on the potential PCMI phase of the accident. High temperature cladding failure due to departure from nucleate boiling in PWRs or dryout in BWRs is beyond the scope of this paper. The mechanical behaviors of both irradiated and unirradiated cladding are established with both integral and separate-effects tests. While integral tests are important for the establishment of the acceptance criteria of ATF candidates for RIA, separate-effects testing is important to inform the integral testing parameters and modeling efforts for the candidate ATF claddings. To this end, the modified burst test (MBT) was developed as one of the separate-effects tests because it can impose loading conditions relevant to RIA.

2. Methodology

In this effort, the previously demonstrated pulse-controlled (PC) MBT technique was used to determine the failure hoop strain for LWR hot zero power (HZP) RIA conditions for FeCrAl cladding material. The MBT technique, which leverages an Inconel driver tube pressurized using oil to burst the cladding samples, was first developed [7] and validated [8] by the Electric Power Research Institute. MBT has been demonstrated to simulate the strain-driven conditions at RIA-relevant timescales.

The PC MBT is an extension of the MBT technique which was developed at Oak Ridge National Laboratory (ORNL) [9] to allow precise control and variation in strain rate and was used later to enable high-fidelity measurement of failure strain using digital image correlation (DIC) techniques. This PC MBT technique was validated [9] against data from historical Penn State plane-strain tension (PST) tests [10] for hydrogen-charged zirconium-based cladding. The agreement between PC MBT and PST test results for the zirconium samples was excellent. The precise control of the PC MBT aims to elucidate the impact of the strain rate on the failure of the cladding and to be capable of simulating RIA scenarios over a range of power pulse widths. This enables a capability for separate-effects tests to connect results from different transient test reactors, including the Transient Reactor Test (TREAT) facility in the United States, CABRI in France, and the Nuclear Safety Research Reactor (NSRR) in Japan.

Originally the PC MBT used strain gauges for instrumentation, which presented challenges because they would only measure the strain at one location of the tube, and they would occasionally detach. Additionally, they posed a challenge when used for elevated temperature tests. To resolve this, a DIC instrumentation system was developed for the PC MBT, and the uncertainties in the DIC technique were thoroughly characterized [11]. The uncertainty in the DIC-measured failure hoop strain was determined to be typically less than 0.05% strain and was always less than 0.1% strain. Most recently, the PC MBT technique was used to define a preliminary safety limit for silicon carbide fiber/silicon carbide matrix (SiC/SiC) cladding based on fuel energy deposition of approximately 50 cal/g-UO_2, assuming initial pellet-cladding contact [12]. The failure strains of SiC/SiC samples tested at slow strain rates showed good agreement with the values reported in the literature, but the specialized capabilities of the PC MBT to produce specific strain rates also enabled identification of a strain rate dependence of the failure hoop strain.

In this effort, the failure strains of fresh FeCrAl cladding samples were determined at strain rates and temperatures relevant to HZP RIA using the well-established PC MBT technique with a DIC

instrumentation system with very well-characterized uncertainties. The quasi-static fuel energy deposition that would cause such a strain was identified, ignoring the potential impact of fission gas within the fuel on that thermal expansion. Finally, the potential strain rate effect of the RIA was studied. This is important because the hardened spectrum in a FeCrAl-clad reactor would shorten the neutron generation time and increase the strain rate of the cladding during PCMI by about 20% relative to zirconium-based cladding during a postulated RIA [3], as shown in Figure 2. These power pulses were calculated for an AP1000-like core design using the regulatory-grade Purdue Advanced Reactor Core Simulator (PARCS).

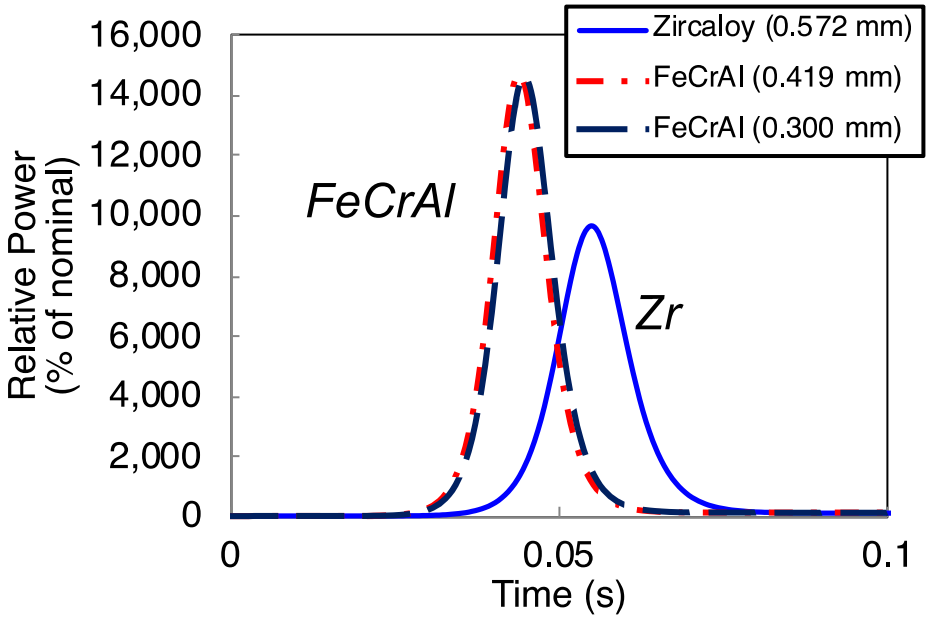

Figure 2. Example power pulses calculated for an HZP RIA in a modern PWR for zirconium-based cladding and two FeCrAl equilibrium core designs with two different cladding thicknesses. These power pulses are representative of a postulated RIA and correspond to cladding strain rates between 0.4 and 0.6 s^{-1}.

The PC MBT testing was performed on FeCrAl tube cladding samples (see Table 1). The modified burst test was performed at 275°C on as-drawn nuclear-grade C26M alloy, which is similar in composition to the LTRs in the Hatch BWR. The tube specimens had a nominal outer diameter of 9.48 mm and a wall thickness of 0.39 mm. The average grain size was 30 microns. A schematic of the setup for the DIC instrumentation is shown in Figure 3, and a photograph of the experimental setup is presented in Figure 4.

Table 1. Composition of the nuclear grade FeCrAl tube samples.

Alloy	Fe	Cr	Al	Mo	Si	Yt	Other
C26M	Bal.	12	6.22	1.98	0.2	0.03	<0.01 C <0.05 S

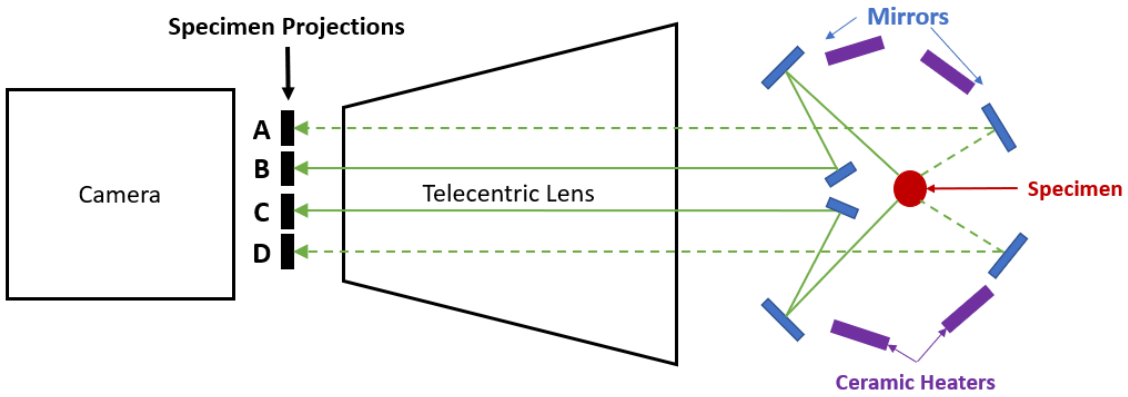

Figure 3. Telecentric lens setup used for the PC MBT DIC instrumentation in these tests.

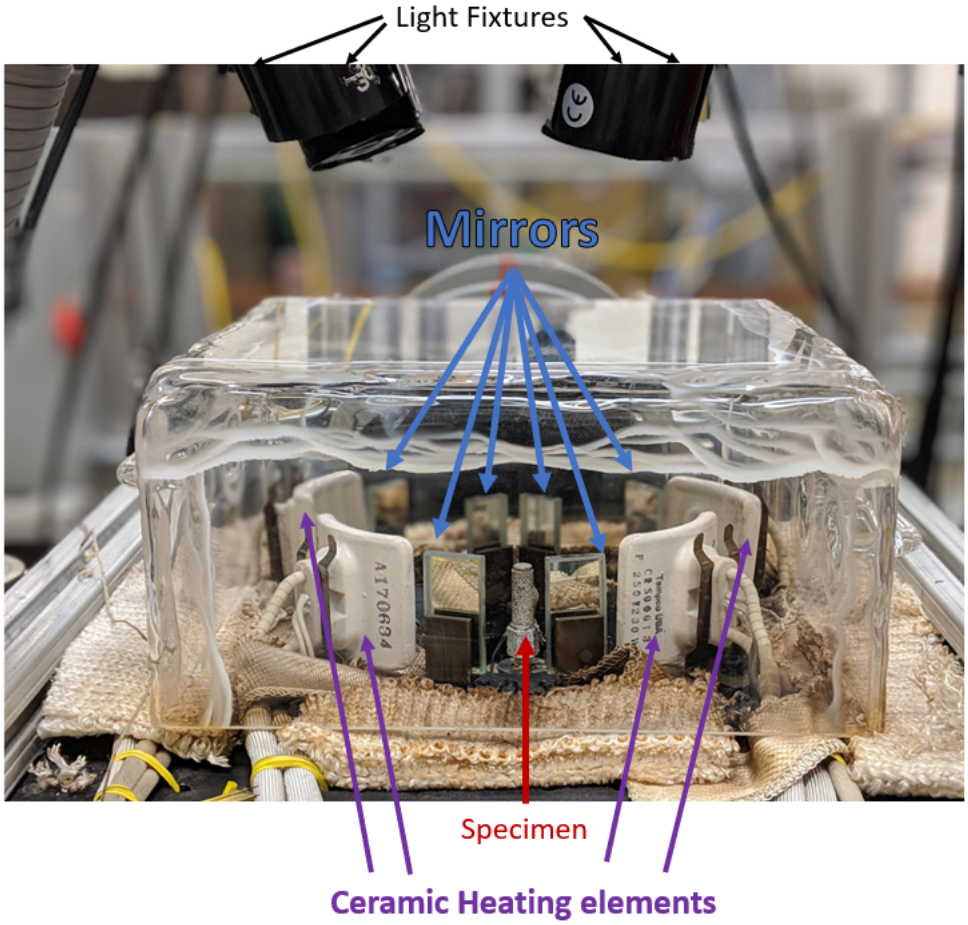

Figure 4. Experimental setup showing the specimen, heating elements, mirrors, and quartz case.

Figure 5 plots a typical pressurization event during MBT. The specimen was pressurized at 9.4 GPa/s corresponding to a calculated strain rate of 5.4 s^{-1}, based on DIC results. The error in the pressure measurement is approximately 1 MPa, and the error bars for the DIC-measured hoop strain indicate a maximum expected value of 0.1%. Before the pressurization event, specimens were heated until the surface temperature reached 275°C. This temperature was achieved by enclosing the mirrors, specimen, and ceramic heating elements in a quartz case and covering the

quartz with fiberglass insulating strips. The temperature was measured by a K-type thermocouple that was wrapped around the bottom of the specimen. Once the test temperature was reached, the insulating strips were removed so the specimen projections were not obstructed, and the specimens were subjected to various pressurization rates to investigate the effect of strain-rate on specimen deformation. The quartz case remained over the setup for the entire test. The driver tube was sealed to the hydraulic system's high-pressure fitting with O-rings.

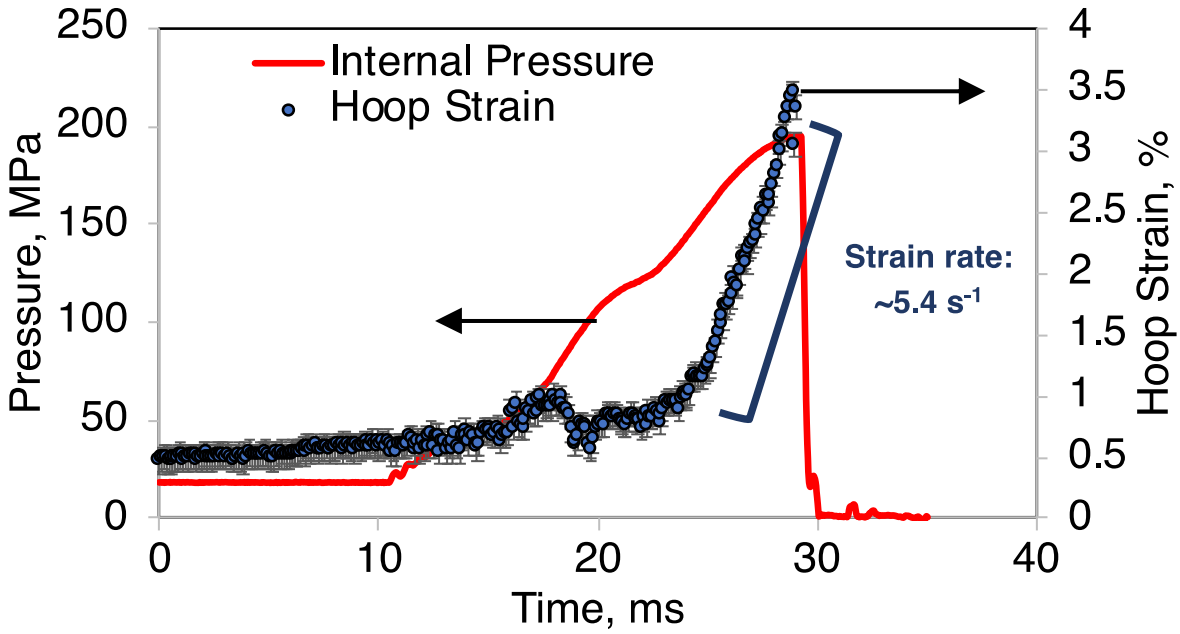

Figure 5. Pressurization event and measure hoop strain during a PC MBT.

The telecentric lens, high-speed camera, and mirror setup described in an earlier report [13] were used to observe the deformation behavior around the entire circumference of the tube's outer surface. Figure 6 shows the pattern wrapped around the tube's surface and the four frames captured with the MBT setup. During the test, mechanical strains were calculated with the established [13] DIC technique using a speckle pattern painted on the specimen surfaces.

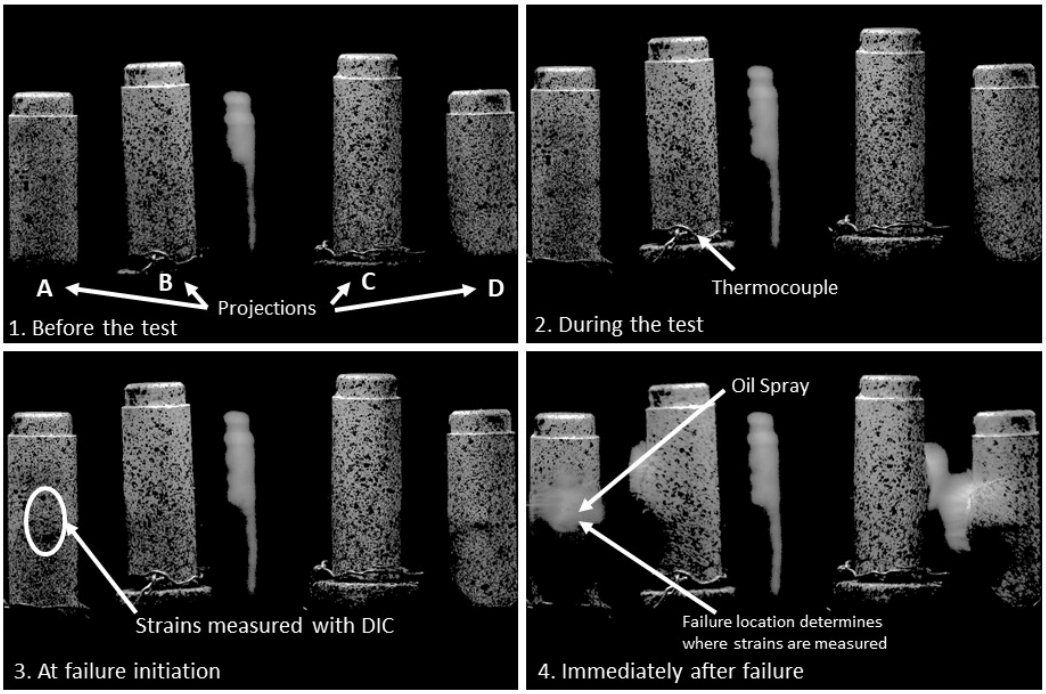

Figure 6. Images from an example MBT experiment. The four projections of the same sample produced a 360° view of the tube's surface.

3. Results and Discussion

A total of six C26M tube specimens were tested with a consistent experimental setup and geometry (nominal outer diameter of 9.48 mm and a wall thickness of 0.39 mm). The MBT setup with 360° DIC measurement allowed for successful calculation of the strain at the failure locations for all six of the burst specimens. These failure strains from MBT were in the expected range for FeCrAl material based on previous preliminary tests [13].

The failure strain was determined by locating the tube's failure location from observing the hydraulic oil spray on the image immediately after the burst occurred (see Figure 6.4). Once the failure location was isolated, the DIC software was used to determine the strain at a few points co-located with the failure location. A summary of the six tests is shown in Table 2. Maximum and minimum strain rates calculated as the slope of the hoop strain fit from the DIC results are reported. Failure strains ranged from 1.8 to 3.4%. These strain rates correspond to those obtained from unconstrained quasi-static thermal expansion of a UO_2 fuel pellet for energy depositions of approximately 110–260 calories per gram UO_2 assuming initial pellet-cladding contact, details of the calculation procedures are reported elsewhere [3, 12]. These quasi-static cladding heat up calculations use the MATPRO correlation for UO_2 thermal expansion and the assumptions were consistent with those used in [3]. At strain rates most relevant to a postulated HZP RIA, the failure strain was about 3.0%. Given the proposed energy deposition limit of 150 calories per gram UO_2 for fresh zirconium-based cladding specified in DG-1327, the expected limits for fresh FeCrAl would likely be similar.

Table 2. Results from the PC MBT tests with C26M FeCrAl alloy at 275°C.

Pressurization rate (GPa/s)	Failure strain (%)	Strain state ratio (-)	Min hoop strain rate (s^{-1})	Max hoop strain rate (s^{-1})	Max pressure (MPa)
0.3	2.9	0.040	0.47	1.1	175
1.5	2.9	0.18	1.0	3.7	174
3.2	2.7	0.14	2.5	6.9	178
6.4	3.4	0.070	3.0	9.4	194
7.7	1.8	0.15	1.6	13.0	173
8.75	2.1	0.14	2.8	18.0	183

Data from a typical test immediately before the time of the tube burst is shown in Figure 7. Exponential least squares fits indicate the trend in each dataset. The error bars on the hoop strain and axial strain are taken from a previous study on the DIC technique [11], conservatively assuming the maximum error of 0.1% strain from that study. The error in the DIC-measured strains was propagated to the biaxiality ratio, which is the minor-to-major strain state ($\varepsilon_2/\varepsilon_1$) ratio. The biaxiality at failure in this example test was approximately 0.14 ± 0.05.

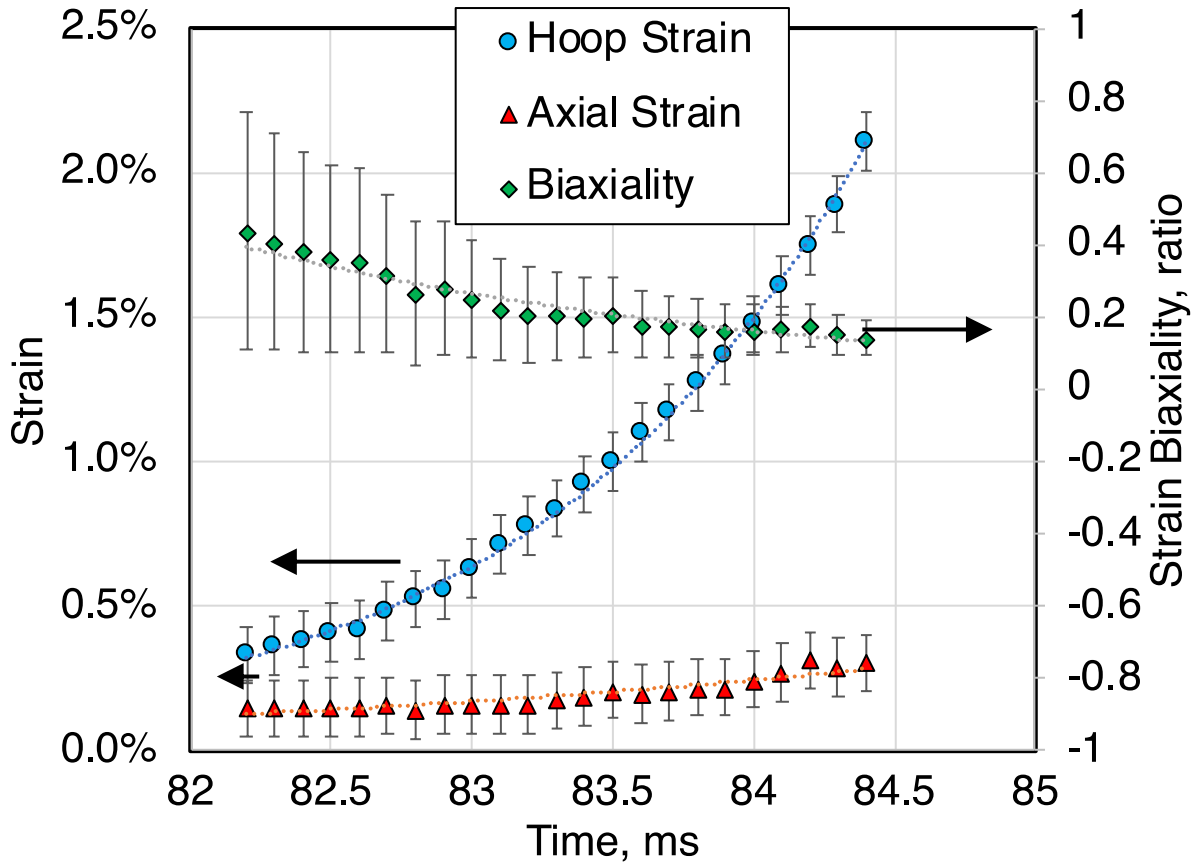

Figure 7. Strain and minor-to-major strain state ($\varepsilon_2/\varepsilon_1$) ratio for the example test with a pressurization rate of 8.75 GPa/s.

The failure hoop strain and biaxiality ratio of each case are plotted in Figure 8. A slight decreasing trend is seen with increasing strain rate. However, all failure strains are within a similar range, and the observed trend is small, so it is difficult to conclusively state the magnitude of the strain rate effect. Tests with residual strain biaxiality ratios >0.1 are shown with a filled marker, and tests with residual strain only in the hoop direction are shown with an empty marker. The residual strain ratios are similar to those presented in Reference 6 for Nuclear Safety Research Reactor (NSRR) tests conducted in Japan.

The two tests with residual strain that was essentially present only in the hoop direction had the two highest failure strains, and the tests with residual strain in both the hoop and axial directions (with a typical residual strain biaxiality of 0.14-0.20 ± 0.05 for all biaxial tests) had slightly lower failure strains. We hypothesize that the lower residual biaxiality may have resulted in higher failure strain, although this hypothesis will require further testing for confirmation. The close correlation between pressurization rate and maximum strain rate experienced during the test is shown in Figure 9. Since the strain rates are calculated from the best-fit curves, the uncertainty in strain rate was calculated assuming it followed a Gaussian distribution.

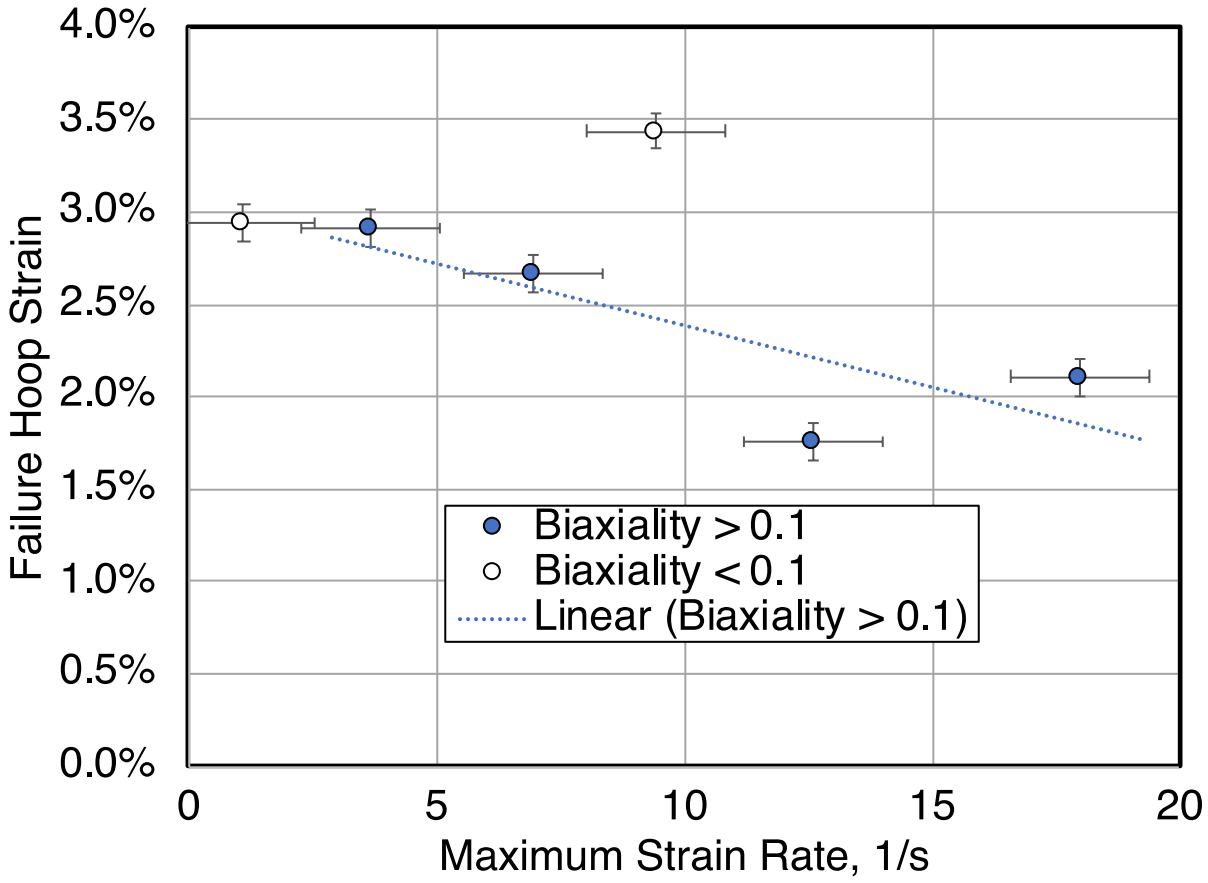

Figure 8. Failure hoop strain as a function of maximum strain rate. The least-squares fit is included only to show the general trend in behavior.

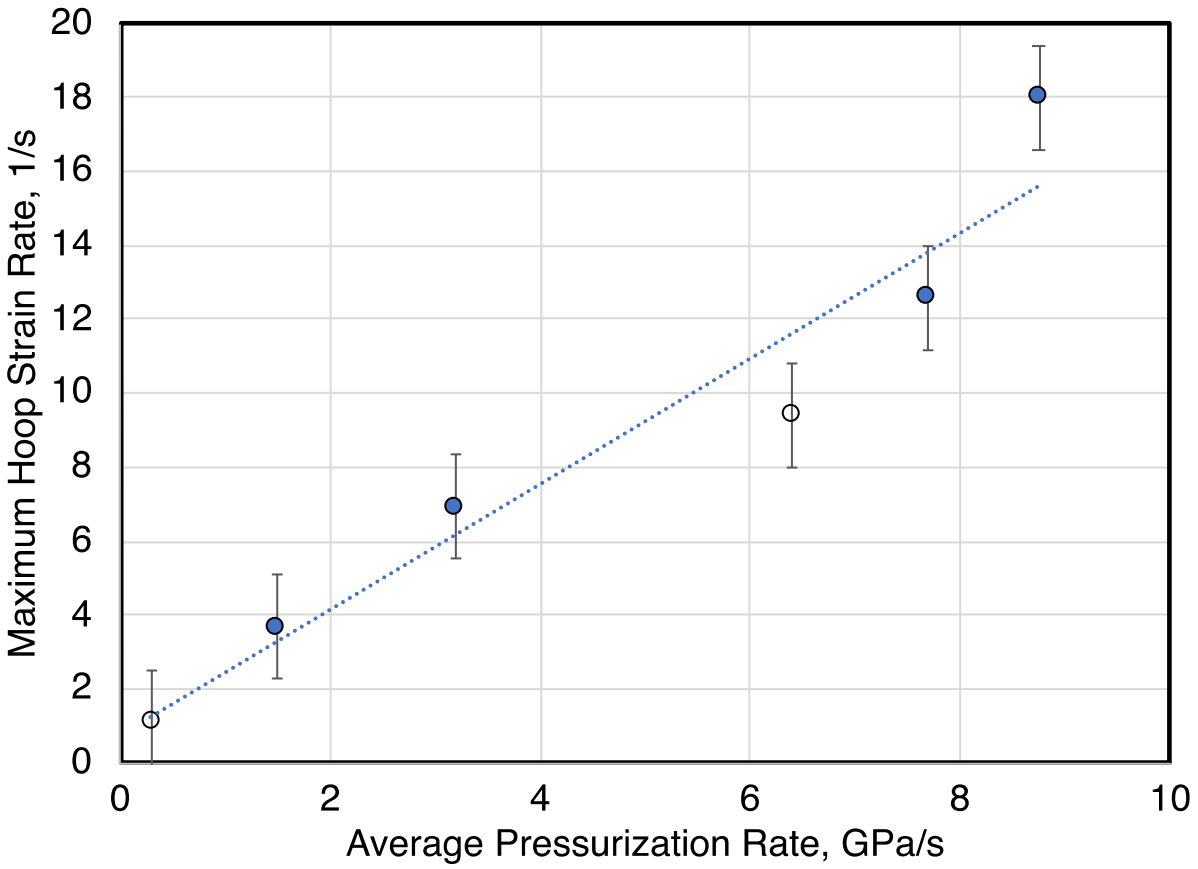

Figure 9. Maximum hoop strain rate experienced within a test vs. the average pressurization rate (shown with a linear fit to illustrate the trend).

To ascertain further information about the fracture behavior scanning electron microscope (SEM) images of the fracture surface were obtained for the two FeCrAl samples with strain rates from 1.0 to 3.7 s^{-1} and 1.6 to 13.0 s^{-1}. These SEM images are shown in Figure 10. Figures 10a and b show fractography of selected samples subjected to low and high strain-rates, respectively. Ductile dimples were observed in all samples, which indicates void initiation, growth, and coalescence behavior governs the mechanical damage process. Ductile dimples were more elongated along the circumference direction for low strain-rate sample while those were elongated along the axial direction for the high strain-rate sample. For the high strain-rate sample, small flat facets on the fracture surface were also noted in addition to the ductile dimples. These observations suggest the strain-rate or the strain-driven nature of the test had an impact since both samples were under similar biaxial loading conditions (see Table 2).

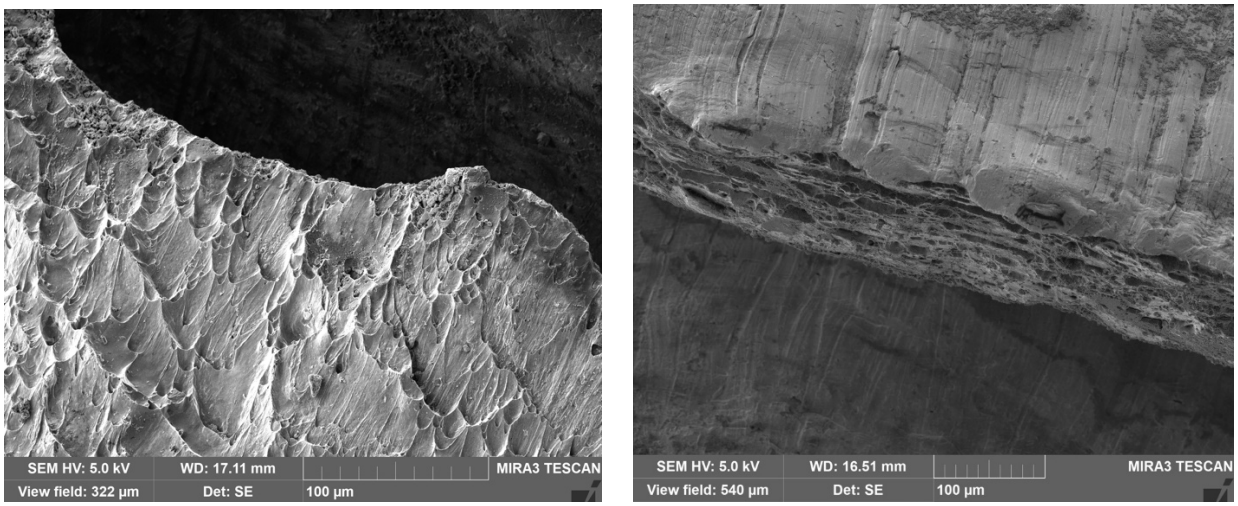

(a) (b)

Figure 10. Fracture surface SEM images for FeCrAl sample with strain rates from (a) 3.7 s^{-1} and (b) 13.0 s^{-1}.

4. Conclusions

PC MBT were performed to investigate the failure strain and also the strain-rate dependence of unirradiated C26M nuclear-grade FeCrAl in HZP RIA-relevant conditions. Failure hoop strains were determined for unirradiated FeCrAl cladding at 275°C, which is relevant to HZP RIA. Additional separate effects (in a hot cell) and integral effects tests in TREAT will help inform the potential impact of irradiation on the cladding failure strain. The measured failure hoop strains ranged from 1.8 to 3.4%, corresponding to unconstrained quasi-static thermal expansion of a UO_2 fuel pellet for energy depositions of approximately 110–260 calories per gram UO_2. The calculation assumes the pellet and cladding are initially in contact. At strain rates most relevant to a postulated HZP RIA, the failure strain was about 2.5–3.0%. A very slight strain rate dependence was indicated by the results. Failure hoop strains were lower in tests with a higher biaxiality ratio relative to tests with a lower biaxiality ratio. Only one out of six data points had a failure strain less than 2.0%. These failure strains suggest that the energy deposition limits for FeCrAl would be similar to those proposed in DG-1327 for unirradiated fuel [5]. The failure limit parametrized as a function of burnup could look very different as the mechanical properties of FeCrAl evolve.

It is notable that the PCMI limit is not the only relevant cladding performance limit during RIA for FeCrAl cladding. The cladding may also fail during the high temperature phase caused by a boiling crisis (e.g. departure from nucleate boiling in a PWR). There are observed differences in measured critical heat flux with FeCrAl cladding [14-16], but these phenomena are outside the scope of the present article. Nevertheless, they would influence the potential energy deposition limits for FeCrAl cladding in LWRs.

Microstructural analyses are recommended to gain further understanding of the fracture mechanisms. Additional testing without the internal Inconel driver tube is recommended for future work to determine if strain-rate dependence of Inconel impacted the tube specimen's strain-rate dependence. Furthermore, future work will involve developing a technique that is relevant to RIA

performance and can more easily be performed in a hot cell so irradiated material can be tested. The separate effects tests performed in this work directly inform the development of potential integral tests of FeCrAl at the TREAT reactor. Information about bonding between FeCrAl and UO_2 at high burnup, which would influence pellet cladding contact and the loading path during the PCMI phase of RIA, will potentially be provided by post irradiation examination of ongoing irradiation experiments with fueled FeCrAl cladding.

5. Acknowledgments

This research was sponsored by the US Department of Energy Office of Nuclear Energy Advanced Fuels Campaign.

Dr. Nathan Capps and Dr. Aaron Wysocki are acknowledged for their excellent internal review comments on the manuscript.

All authors contributed significantly to this manuscript and the PC MBT effort at ORNL over the past five years. N. R. Brown prepared the draft of the manuscript, helped design the original experimental facility, helped develop the analysis methodology for the current dataset, and provided the relevance to postulated RIA. B. E. Garrison conducted the experiments, analyzed the data, and provided input to the manuscript. R. R. Lowden set up the PC MBT fixtures and assisted in conducting the experiments. M. N. Cinbiz helped design the original experimental facility, developed the DIC instrumentation system, planned the test matrix for these tests, and provided input to the manuscript. K. D. Linton provided the management and coordination for execution of the overall project and provided input to the manuscript.

6. References

[1] Le Coq, A.G., R.C. Martin, and K. Linton, Transportation Planning for Irradiated Fuel-Clad and Integral FeCrAl Experiments, *ORNL/TM-2019/1123*, 2019, Oak Ridge National Laboratory (ORNL), Oak Ridge, TN (United States).

[2] Rebak, R.B., Iron-chrome-aluminum alloy cladding for increasing safety in nuclear power plants. *EPJ Nucl. Sci. Technol.* 3 (2017) 34.

[3] Brown, N.R., A.J. Wysocki, K.A. Terrani, K.G. Xu, and D.M. Wachs, The potential impact of enhanced accident tolerant cladding materials on reactivity initiated accidents in light water reactors. *Ann. Nucl. Energy* 99 (2017) 353–365.

[4] Ott, K.O. and Neuhold, R.J., 1985. *Introductory nuclear reactor dynamics*. American Nuclear Society.

[5] U.S. Nuclear Regulatory Commission, DG-1327, "Pressurized Water Reactor Control Rod Ejection and Boiling Water Reactor Control Rod Drop Accidents", Nov. 2016, (ADAMS Accession No. ML16124A200)

[6] Desquines, J., Koss, D.A., Motta, A.T., Cazalis, B., Petit, M., The issue of stress state during mechanical tests to assess cladding performance during a reactivity-initiated accident (RIA). *Journal of Nuclear Materials,* 412 (2011) 250-267.

[7] Yueh, K., Karlsson, J., Stjärnsäter, J., Schrire, D., Ledergerber, G., Munoz-Reja, C. and Hallstadius, L., 2016. Fuel cladding behavior under rapid loading conditions. *Journal of Nuclear Materials*, *469*, pp.177-186.

[8] Yueh, K., 2017. Applicability of modified burst test data to reactivity initiated accident. *Journal of Nuclear Materials*, *488*, pp.338-345.
[9] Cinbiz, M.N., Brown, N.R., Terrani, K.A., Lowden, R.R. and Erdman III, D., 2017. A pulse-controlled modified-burst test instrument for accident-tolerant fuel cladding. *Annals of Nuclear Energy*, *109*, pp.396-404.
[10] Link, T.M., Koss, D.A. and Motta, A.T., 1998. Failure of Zircaloy cladding under transverse plane-strain deformation. *Nuclear Engineering and Design*, *186*(3), pp.379-394.
[11] Cinbiz, M.N., Gussev, M., Linton, K. and Terrani, K.A., 2019. An advanced experimental design for modified burst testing of nuclear fuel cladding materials during transient loading. *Annals of Nuclear Energy*, *127*, pp.30-38.
[12] Cinbiz, M.N., Koyanagi, T., Singh, G., Katoh, Y., Terrani, K.A. and Brown, N.R., 2019. Failure behavior of SiC/SiC composite tubes under strain rates similar to the pellet-cladding mechanical interaction phase of reactivity-initiated accidents. *Journal of Nuclear Materials*, *514*, pp.66-73.
[13] M. N. Cinbiz, N. R. Brown, R. R. Lowden, M. Gussev, K. Linton, K. A. Terrani. *Report on Design and Failure Limits of SiC/SiC and FeCrAl ATF Cladding Concepts under RIA*, July 2018, ORNL/LTR-2018/521.
[14] Ali, A.F., Gorton, J.P., Brown, N.R., Terrani, K.A., Jensen, C.B., Lee, Y. and Blandford, E.D., 2018. Surface wettability and pool boiling critical heat flux of accident tolerant fuel cladding-FeCrAl alloys. *Nuclear engineering and design*, *338*, pp.218-231.
[15] Lee, S.K., Liu, M., Brown, N.R., Terrani, K.A., Blandford, E.D., Ban, H., Jensen, C.B. and Lee, Y., 2019. Comparison of steady and transient flow boiling critical heat flux for FeCrAl accident tolerant fuel cladding alloy, Zircaloy, and Inconel. *International Journal of Heat and Mass Transfer*, *132*, pp.643-654.
[16] Gorton, J.P., Lee, S.K., Lee, Y. and Brown, N.R., 2019. Comparison of experimental and simulated critical heat flux tests with various cladding alloys: Sensitivity of iron-chromium-aluminum (FeCrAl) to heat transfer coefficients and material properties. *Nuclear Engineering and Design*, *353*, p.110295.

Mechanical Failure of Fresh Nuclear Grade Iron-Chromium-Aluminum (FeCrAl) Cladding Under Simulated Hot Zero Power Reactivity Initiated Accident Conditions[†]

Nicholas R. Brown[1,*], Benton E. Garrison[2,*], Richard R. Lowden[2], M. Nedim Cinbiz[2,3], Kory D. Linton[2]

[1] University of Tennessee-Knoxville, Knoxville, TN 37913
[2] Oak Ridge National Laboratory, Oak Ridge, TN 37830
[3] Present affiliation: Idaho National Laboratory, Idaho Falls, ID 83402

* The authors N. R. Brown and B. E. Garrison are considered co-first authors and equal contributors to this manuscript. Corresponding author: nbrown49@utk.edu (N. R. Brown)

Abstract

The reactivity initiated accident (RIA) is a postulated accident in light water reactors initiated by a rapid increase in reactivity which causes an increase in fission rate and fuel temperature. One potential mode of fuel system failure during RIA is pellet cladding mechanical interaction (PCMI) due to the rapid thermal expansion of the fuel pellet. Simulated PCMI experiments were performed by rapidly pressurizing cladding tube samples using a hydraulic modified burst test system, causing the specimens to burst under a biaxial loading path. Deformation and rupture of the specimens were tracked with a telecentric lens and high-speed camera system. Outer surface strains were calculated using digital image correlation (DIC) on speckle patterns painted on the specimens' outer surfaces. Experiments were conducted at approximately 275°C, representative of hot zero power RIA conditions. The failure hoop strain was DIC-calculated between approximately 1.8–3.4%, corresponding to quasi-static energy depositions of approximately 110–260 calories per gram UO_2 assuming initial pellet-cladding contact. These conditions are very similar to the proposed energy deposition limit of 150 calories per gram UO_2 for unirradiated zirconium-based cladding in US Nuclear Regulatory Commission (NRC) Draft Regulatory Guide 1327. A very small strain rate dependence was observed in the data, with the magnitude of the failure hoop strain decreasing slightly with increasing strain rate. This observed dependence may be relevant because the iron-chromium-aluminum (FeCrAl) cladding strain rate will be approximately 20% higher than in zirconium-based cladding due to the harder neutron spectrum and resultant shorter neutron generation time.

1. Introduction

Nuclear-grade iron-chromium-aluminum (FeCrAl) cladding alloy C26M, a leading candidate for *IronClad*™ [1], has been established as a leading candidate accident-tolerant fuel (ATF) cladding material [2]. FeCrAl cladding is currently being irradiated as lead test rods (LTRs) in the Hatch

---

[†] This manuscript has been co-authored by UT-Battelle, LLC, under contract DE-AC05-00OR22725 with the US Department of Energy (DOE). The US government retains and the publisher, by accepting the article for publication, acknowledges that the US government retains a nonexclusive, paid-up, irrevocable, worldwide license to publish or reproduce the published form of this manuscript, or allow others to do so, for US government purposes. DOE will provide public access to these results of federally sponsored research in accordance with the DOE Public Access Plan (http://energy.gov/downloads/doe-public-access-plan).

Boiling Water Reactor (BWR). The objective of ATF cladding such as FeCrAl is to preserve or improve the current performance and safety characteristics of light-water reactors (LWRs). This includes during a postulated reactivity-initiated accident (RIA) [3]. The primary initiating event considered for RIA is a control rod ejection in a pressurized water reactor (PWR) or a control rod drop in a BWR. This paper presents the results of separate effects tests that were conducted to provide data relevant to establishing safety limits for FeCrAl cladding in postulated RIA events in LWRs. The separate effects test data is also functional for establishing conditions for integral reactivity-initiated accident (RIA) testing in the TREAT reactor at Idaho National Laboratory (INL).

An RIA causes a prompt increase of the fission-rate density in nuclear fuel. Most of the energy associated with the fission-rate density is promptly deposited in the fuel (approximately 90%) [4]. The deposited energy causes the fuel temperature to rapidly increase, and the fuel experiences thermal expansion. During fuel thermal expansion, if the fuel-cladding gap is already closed or closes during RIA, the expansion of fuel induces mechanical strain on the cladding. This is known as the pellet-cladding mechanical interaction (PCMI) phase of the RIA. In a super prompt RIA, the events can occur with pulse widths as short as tens of milliseconds (see Figure 1). The event is terminated by prompt inherent feedback (i.e., the Doppler coefficient in an LWR). If the mechanical strain on the cladding is sufficient, the cladding may rupture. US Nuclear Regulatory Commission (NRC) Draft Regulatory Guide 1327 (DG-1327) presents energy deposition limits expressed as total peak radial average fuel enthalpy increase in calories per gram UO_2 for zirconium-based cladding [5]. These limits indicate that cladding failure is expected at 150 calories per gram UO_2 for several types of fresh zirconium-based cladding.

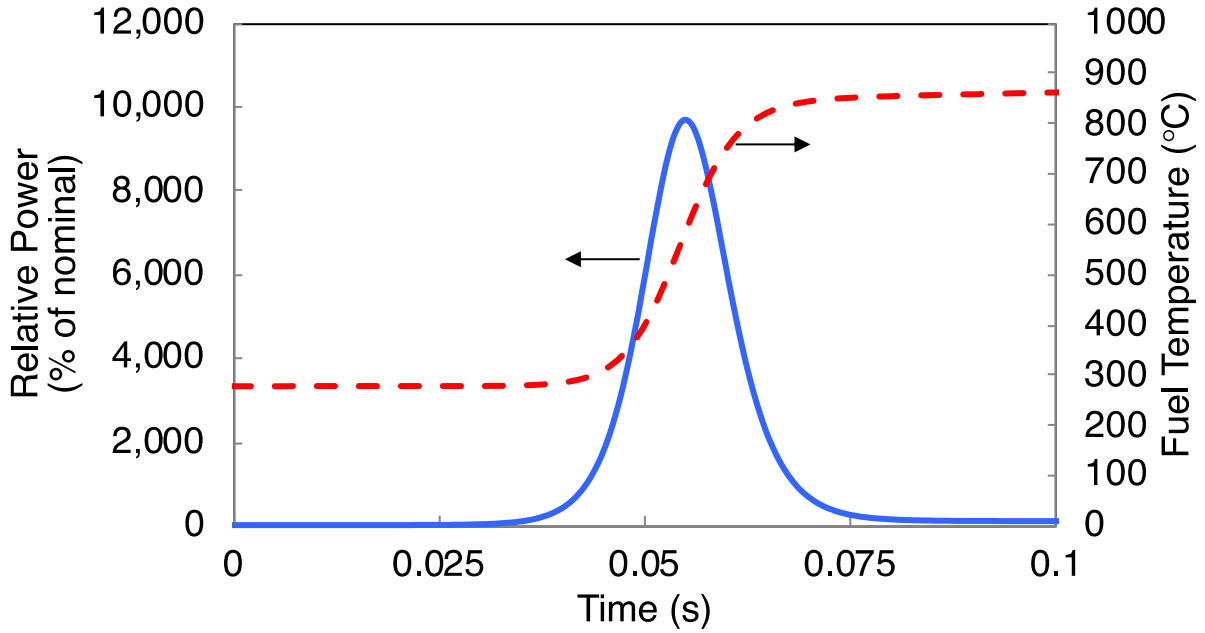

Figure 1. Example RIA showing the prompt increase in fission rate that is terminated by the prompt inherent feedback.

RIA imposes special mechanical loading conditions on the cladding tubes. Under RIA PCMI, cladding tubes are expected to be under a multiaxial and strain-driven loading condition with strain rates of 1–5 s^{-1} [6]. This paper is focused on the potential PCMI phase of the accident. High temperature cladding failure due to departure from nucleate boiling in PWRs or dryout in BWRs is beyond the scope of this paper. The mechanical behaviors of both irradiated and unirradiated cladding are established with both integral and separate-effects tests. While integral tests are important for the establishment of the acceptance criteria of ATF candidates for RIA, separate-effects testing is important to inform the integral testing parameters and modeling efforts for the candidate ATF claddings. To this end, the modified burst test (MBT) was developed as one of the separate-effects tests because it can impose loading conditions relevant to RIA.

2. Methodology

In this effort, the previously demonstrated pulse-controlled (PC) MBT technique was used to determine the failure hoop strain for LWR hot zero power (HZP) RIA conditions for FeCrAl cladding material. The MBT technique, which leverages an Inconel driver tube pressurized using oil to burst the cladding samples, was first developed [7] and validated [8] by the Electric Power Research Institute. MBT has been demonstrated to simulate the strain-driven conditions at RIA-relevant timescales.

The PC MBT is an extension of the MBT technique which was developed at Oak Ridge National Laboratory (ORNL) [9] to allow precise control and variation in strain rate and was used later to enable high-fidelity measurement of failure strain using digital image correlation (DIC) techniques. This PC MBT technique was validated [9] against data from historical Penn State plane-strain tension (PST) tests [10] for hydrogen-charged zirconium-based cladding. The agreement between PC MBT and PST test results for the zirconium samples was excellent. The precise control of the PC MBT aims to elucidate the impact of the strain rate on the failure of the cladding and to be capable of simulating RIA scenarios over a range of power pulse widths. This enables a capability for separate-effects tests to connect results from different transient test reactors, including the Transient Reactor Test (TREAT) facility in the United States, CABRI in France, and the Nuclear Safety Research Reactor (NSRR) in Japan.

Originally the PC MBT used strain gauges for instrumentation, which presented challenges because they would only measure the strain at one location of the tube, and they would occasionally detach. Additionally, they posed a challenge when used for elevated temperature tests. To resolve this, a DIC instrumentation system was developed for the PC MBT, and the uncertainties in the DIC technique were thoroughly characterized [11]. The uncertainty in the DIC-measured failure hoop strain was determined to be typically less than 0.05% strain and was always less than 0.1% strain. Most recently, the PC MBT technique was used to define a preliminary safety limit for silicon carbide fiber/silicon carbide matrix (SiC/SiC) cladding based on fuel energy deposition of approximately 50 cal/g-UO_2, assuming initial pellet-cladding contact [12]. The failure strains of SiC/SiC samples tested at slow strain rates showed good agreement with the values reported in the literature, but the specialized capabilities of the PC MBT to produce specific strain rates also enabled identification of a strain rate dependence of the failure hoop strain.

In this effort, the failure strains of fresh FeCrAl cladding samples were determined at strain rates and temperatures relevant to HZP RIA using the well-established PC MBT technique with a DIC

instrumentation system with very well-characterized uncertainties. The quasi-static fuel energy deposition that would cause such a strain was identified, ignoring the potential impact of fission gas within the fuel on that thermal expansion. Finally, the potential strain rate effect of the RIA was studied. This is important because the hardened spectrum in a FeCrAl-clad reactor would shorten the neutron generation time and increase the strain rate of the cladding during PCMI by about 20% relative to zirconium-based cladding during a postulated RIA [3], as shown in Figure 2. These power pulses were calculated for an AP1000-like core design using the regulatory-grade Purdue Advanced Reactor Core Simulator (PARCS).

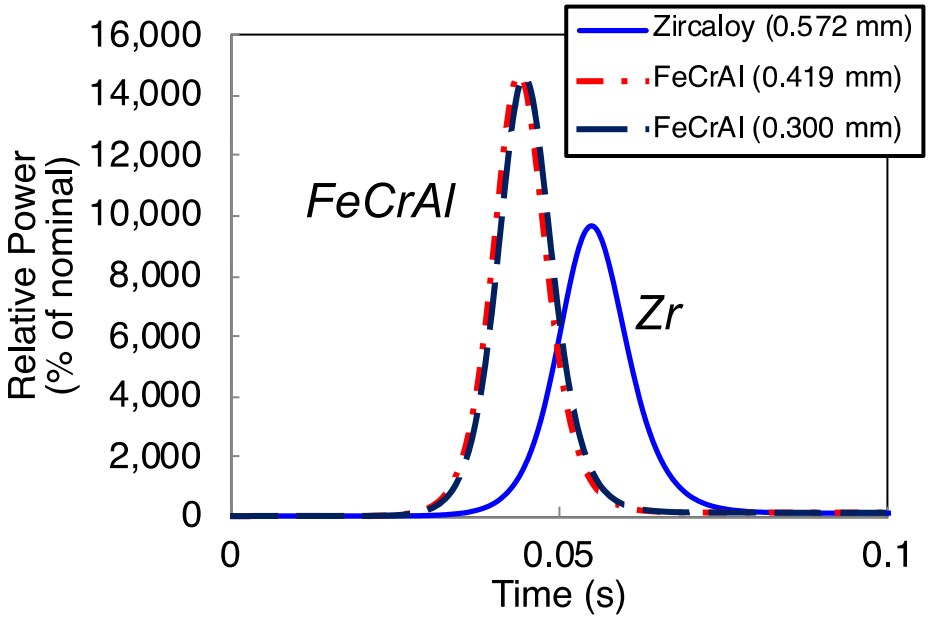

Figure 2. Example power pulses calculated for an HZP RIA in a modern PWR for zirconium-based cladding and two FeCrAl equilibrium core designs with two different cladding thicknesses. These power pulses are representative of a postulated RIA and correspond to cladding strain rates between 0.4 and 0.6 s^{-1}.

The PC MBT testing was performed on FeCrAl tube cladding samples (see Table 1). The modified burst test was performed at 275°C on as-drawn nuclear-grade C26M alloy, which is similar in composition to the LTRs in the Hatch BWR. The tube specimens had a nominal outer diameter of 9.48 mm and a wall thickness of 0.39 mm. The average grain size was 30 microns. A schematic of the setup for the DIC instrumentation is shown in Figure 3, and a photograph of the experimental setup is presented in Figure 4.

Table 1. Composition of the nuclear grade FeCrAl tube samples.

Alloy	Fe	Cr	Al	Mo	Si	Yt	Other
C26M	Bal.	12	6.22	1.98	0.2	0.03	<0.01 C <0.05 S

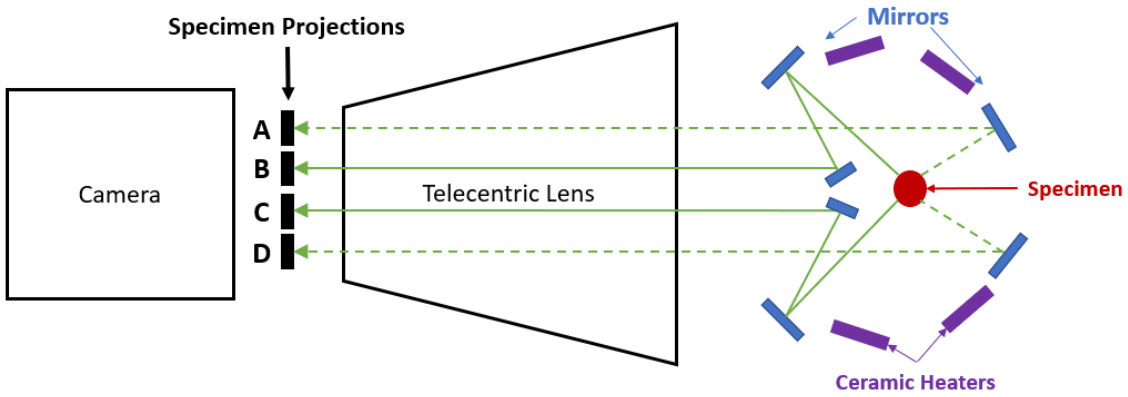

Figure 3. Telecentric lens setup used for the PC MBT DIC instrumentation in these tests.

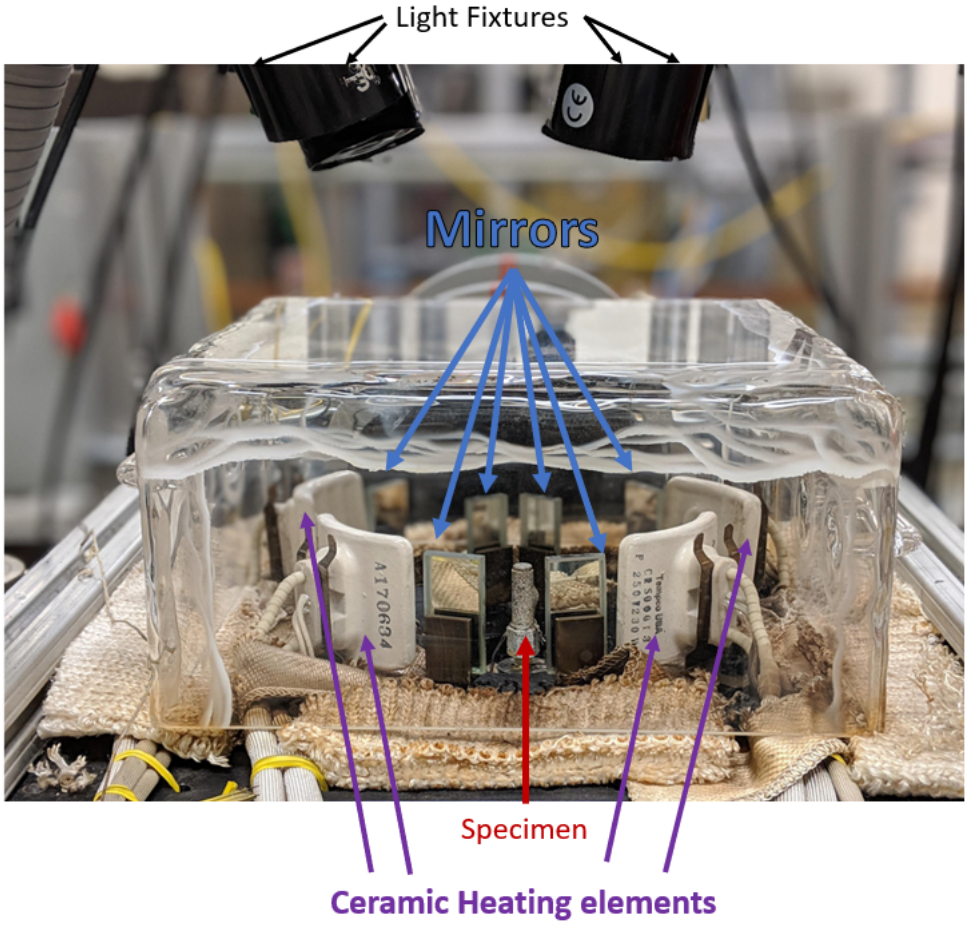

Figure 4. Experimental setup showing the specimen, heating elements, mirrors, and quartz case.

Figure 5 plots a typical pressurization event during MBT. The specimen was pressurized at 9.4 GPa/s corresponding to a calculated strain rate of 5.4 s^{-1}, based on DIC results. The error in the pressure measurement is approximately 1 MPa, and the error bars for the DIC-measured hoop strain indicate a maximum expected value of 0.1%. Before the pressurization event, specimens were heated until the surface temperature reached 275°C. This temperature was achieved by enclosing the mirrors, specimen, and ceramic heating elements in a quartz case and covering the

quartz with fiberglass insulating strips. The temperature was measured by a K-type thermocouple that was wrapped around the bottom of the specimen. Once the test temperature was reached, the insulating strips were removed so the specimen projections were not obstructed, and the specimens were subjected to various pressurization rates to investigate the effect of strain-rate on specimen deformation. The quartz case remained over the setup for the entire test. The driver tube was sealed to the hydraulic system's high-pressure fitting with O-rings.

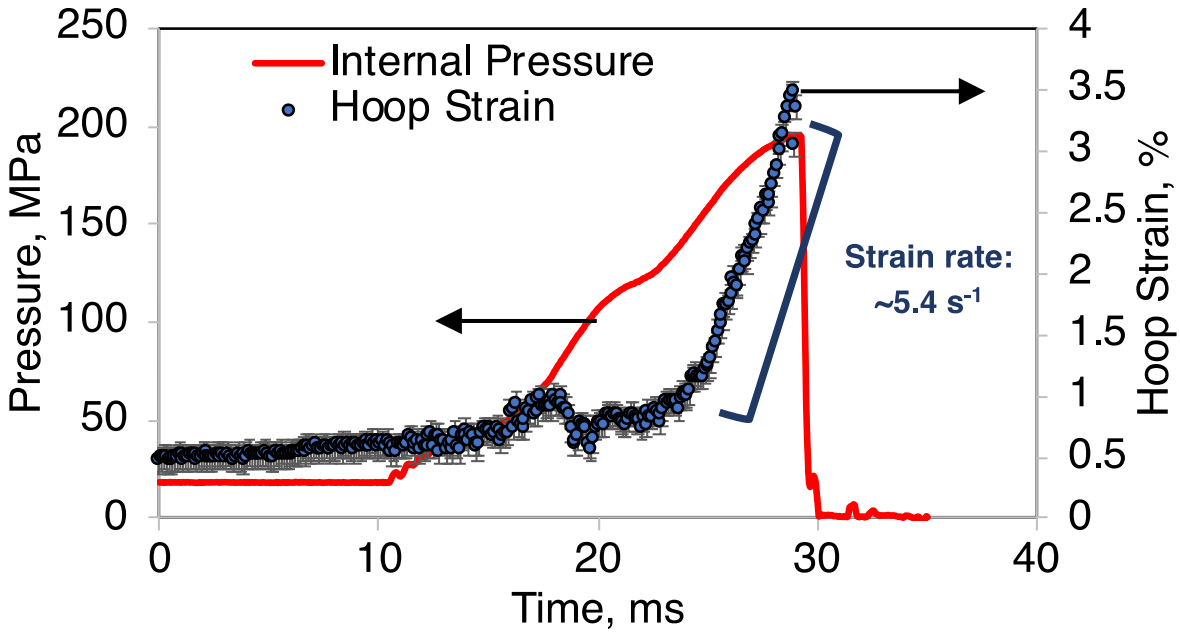

Figure 5. Pressurization event and measure hoop strain during a PC MBT.

The telecentric lens, high-speed camera, and mirror setup described in an earlier report [13] were used to observe the deformation behavior around the entire circumference of the tube's outer surface. Figure 6 shows the pattern wrapped around the tube's surface and the four frames captured with the MBT setup. During the test, mechanical strains were calculated with the established [13] DIC technique using a speckle pattern painted on the specimen surfaces.

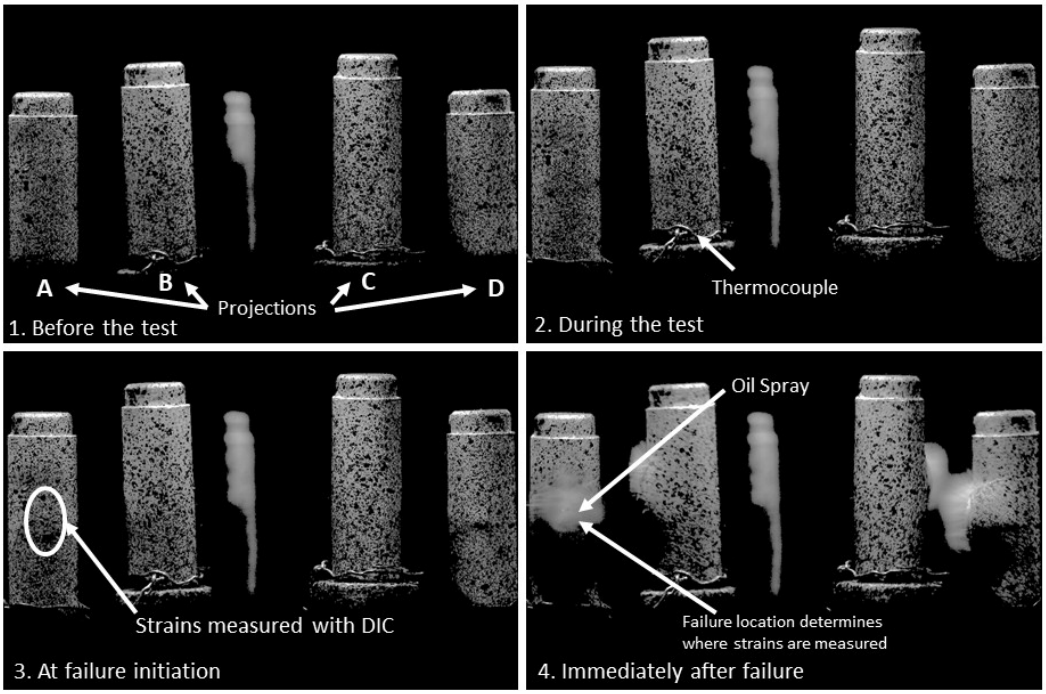

Figure 6. Images from an example MBT experiment. The four projections of the same sample produced a 360° view of the tube's surface.

3. Results and Discussion

A total of six C26M tube specimens were tested with a consistent experimental setup and geometry (nominal outer diameter of 9.48 mm and a wall thickness of 0.39 mm). The MBT setup with 360° DIC measurement allowed for successful calculation of the strain at the failure locations for all six of the burst specimens. These failure strains from MBT were in the expected range for FeCrAl material based on previous preliminary tests [13].

The failure strain was determined by locating the tube's failure location from observing the hydraulic oil spray on the image immediately after the burst occurred (see Figure 6.4). Once the failure location was isolated, the DIC software was used to determine the strain at a few points co-located with the failure location. A summary of the six tests is shown in Table 2. Maximum and minimum strain rates calculated as the slope of the hoop strain fit from the DIC results are reported. Failure strains ranged from 1.8 to 3.4%. These strain rates correspond to those obtained from unconstrained quasi-static thermal expansion of a UO_2 fuel pellet for energy depositions of approximately 110–260 calories per gram UO_2 assuming initial pellet-cladding contact, details of the calculation procedures are reported elsewhere [3, 12]. These quasi-static cladding heat up calculations use the MATPRO correlation for UO_2 thermal expansion and the assumptions were consistent with those used in [3]. At strain rates most relevant to a postulated HZP RIA, the failure strain was about 3.0%. Given the proposed energy deposition limit of 150 calories per gram UO_2 for fresh zirconium-based cladding specified in DG-1327, the expected limits for fresh FeCrAl would likely be similar.

Table 2. Results from the PC MBT tests with C26M FeCrAl alloy at 275°C.

Pressurization rate (GPa/s)	Failure strain (%)	Strain state ratio (-)	Min hoop strain rate (s^{-1})	Max hoop strain rate (s^{-1})	Max pressure (MPa)
0.3	2.9	0.040	0.47	1.1	175
1.5	2.9	0.18	1.0	3.7	174
3.2	2.7	0.14	2.5	6.9	178
6.4	3.4	0.070	3.0	9.4	194
7.7	1.8	0.15	1.6	13.0	173
8.75	2.1	0.14	2.8	18.0	183

Data from a typical test immediately before the time of the tube burst is shown in Figure 7. Exponential least squares fits indicate the trend in each dataset. The error bars on the hoop strain and axial strain are taken from a previous study on the DIC technique [11], conservatively assuming the maximum error of 0.1% strain from that study. The error in the DIC-measured strains was propagated to the biaxiality ratio, which is the minor-to-major strain state ($\varepsilon_2/\varepsilon_1$) ratio. The biaxiality at failure in this example test was approximately 0.14 ± 0.05.

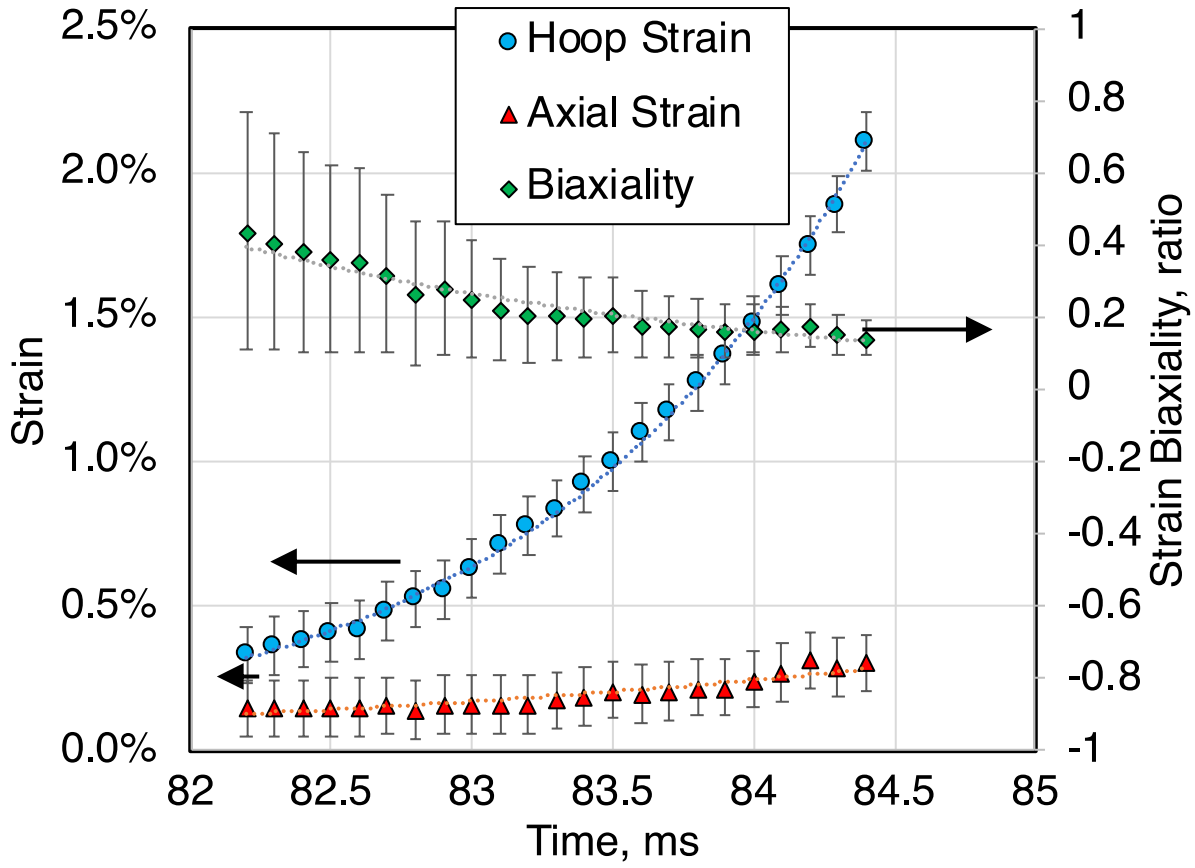

Figure 7. Strain and minor-to-major strain state ($\varepsilon_2/\varepsilon_1$) ratio for the example test with a pressurization rate of 8.75 GPa/s.

The failure hoop strain and biaxiality ratio of each case are plotted in Figure 8. A slight decreasing trend is seen with increasing strain rate. However, all failure strains are within a similar range, and the observed trend is small, so it is difficult to conclusively state the magnitude of the strain rate effect. Tests with residual strain biaxiality ratios >0.1 are shown with a filled marker, and tests with residual strain only in the hoop direction are shown with an empty marker. The residual strain ratios are similar to those presented in Reference 6 for Nuclear Safety Research Reactor (NSRR) tests conducted in Japan.

The two tests with residual strain that was essentially present only in the hoop direction had the two highest failure strains, and the tests with residual strain in both the hoop and axial directions (with a typical residual strain biaxiality of 0.14-0.20 ± 0.05 for all biaxial tests) had slightly lower failure strains. We hypothesize that the lower residual biaxiality may have resulted in higher failure strain, although this hypothesis will require further testing for confirmation. The close correlation between pressurization rate and maximum strain rate experienced during the test is shown in Figure 9. Since the strain rates are calculated from the best-fit curves, the uncertainty in strain rate was calculated assuming it followed a Gaussian distribution.

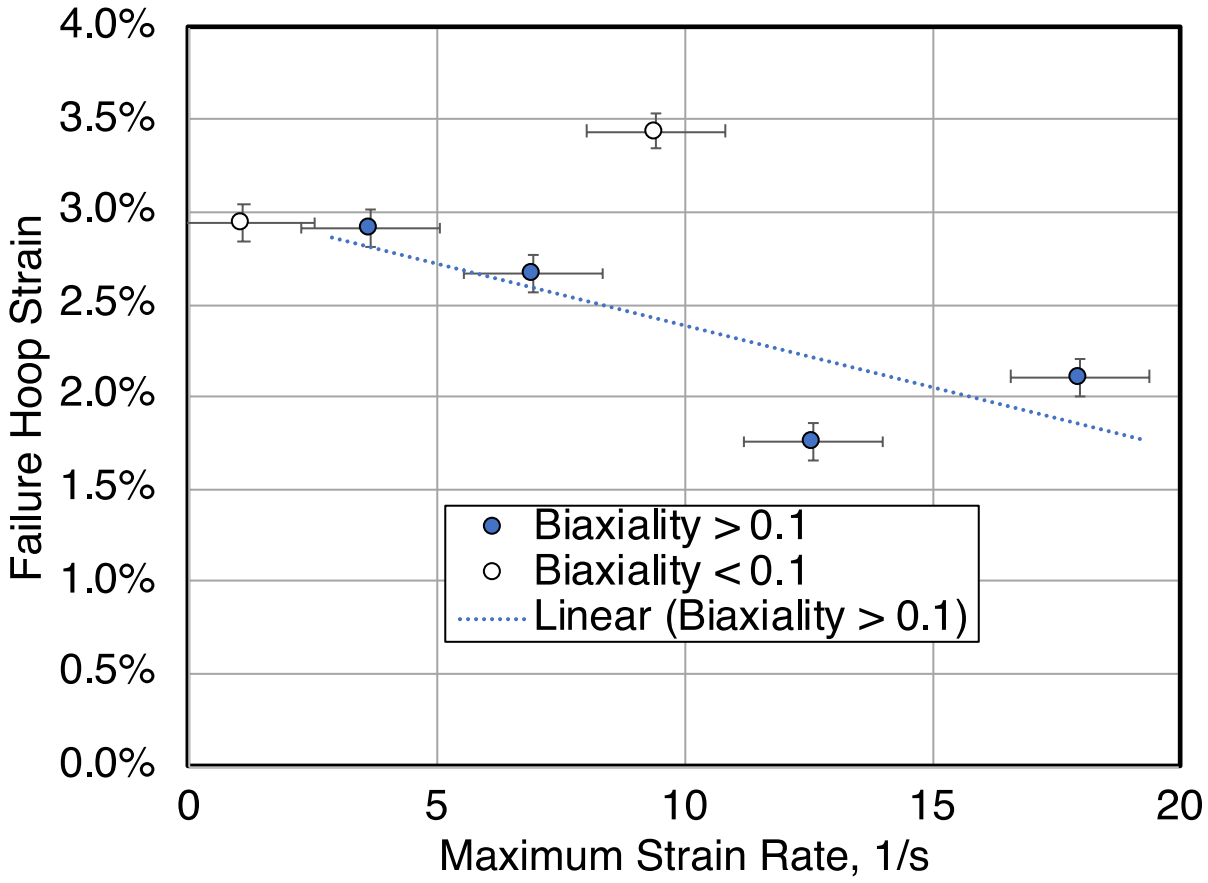

Figure 8. Failure hoop strain as a function of maximum strain rate. The least-squares fit is included only to show the general trend in behavior.

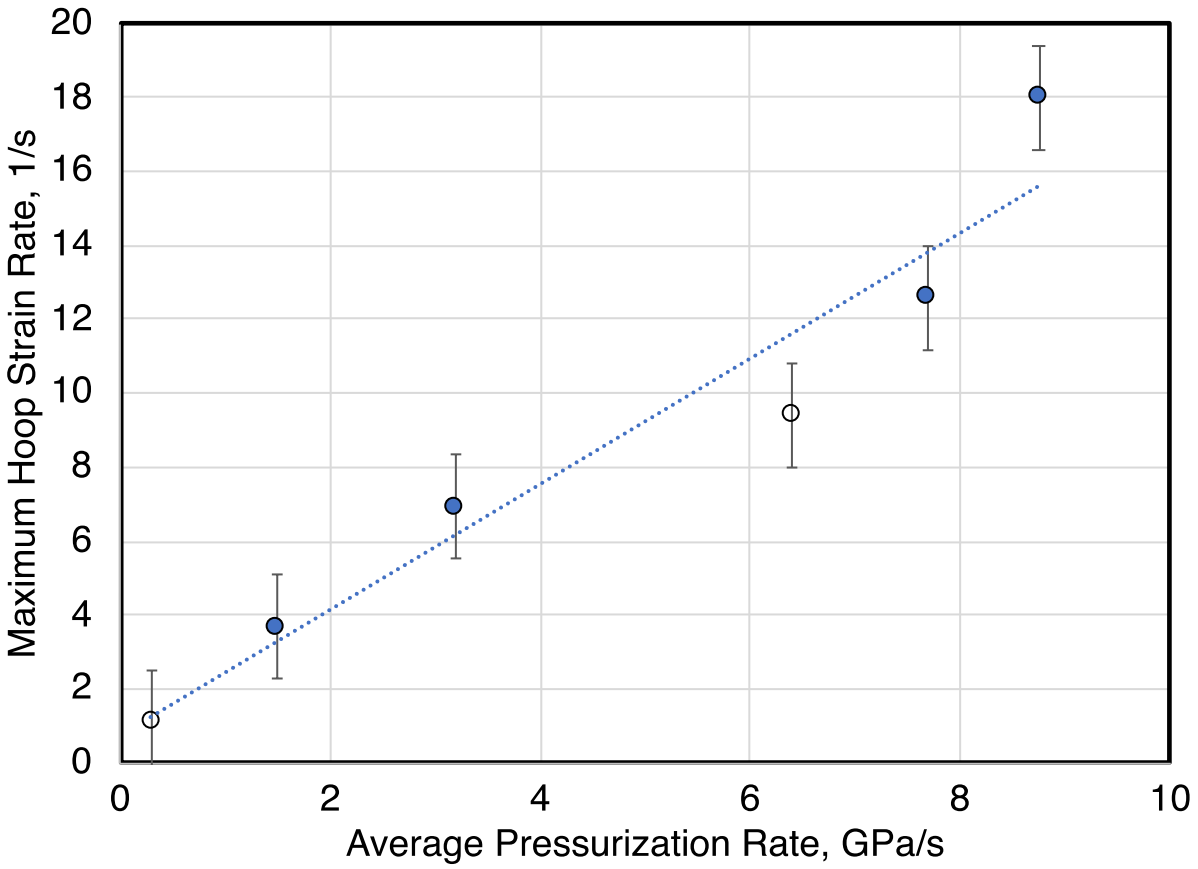

Figure 9. Maximum hoop strain rate experienced within a test vs. the average pressurization rate (shown with a linear fit to illustrate the trend).

To ascertain further information about the fracture behavior scanning electron microscope (SEM) images of the fracture surface were obtained for the two FeCrAl samples with strain rates from 1.0 to 3.7 s^{-1} and 1.6 to 13.0 s^{-1}. These SEM images are shown in Figure 10. Figures 10a and b show fractography of selected samples subjected to low and high strain-rates, respectively. Ductile dimples were observed in all samples, which indicates void initiation, growth, and coalescence behavior governs the mechanical damage process. Ductile dimples were more elongated along the circumference direction for low strain-rate sample while those were elongated along the axial direction for the high strain-rate sample. For the high strain-rate sample, small flat facets on the fracture surface were also noted in addition to the ductile dimples. These observations suggest the strain-rate or the strain-driven nature of the test had an impact since both samples were under similar biaxial loading conditions (see Table 2).

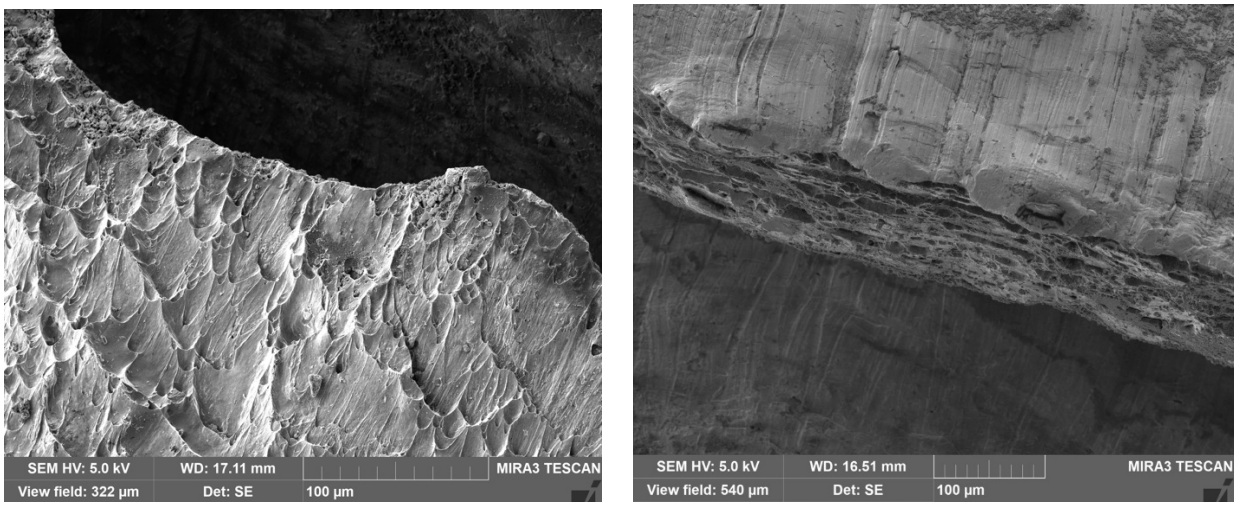

(a) (b)

Figure 10. Fracture surface SEM images for FeCrAl sample with strain rates from (a) 3.7 s^{-1} and (b) 13.0 s^{-1}.

4. Conclusions

PC MBT were performed to investigate the failure strain and also the strain-rate dependence of unirradiated C26M nuclear-grade FeCrAl in HZP RIA-relevant conditions. Failure hoop strains were determined for unirradiated FeCrAl cladding at 275°C, which is relevant to HZP RIA. Additional separate effects (in a hot cell) and integral effects tests in TREAT will help inform the potential impact of irradiation on the cladding failure strain. The measured failure hoop strains ranged from 1.8 to 3.4%, corresponding to unconstrained quasi-static thermal expansion of a UO_2 fuel pellet for energy depositions of approximately 110–260 calories per gram UO_2. The calculation assumes the pellet and cladding are initially in contact. At strain rates most relevant to a postulated HZP RIA, the failure strain was about 2.5–3.0%. A very slight strain rate dependence was indicated by the results. Failure hoop strains were lower in tests with a higher biaxiality ratio relative to tests with a lower biaxiality ratio. Only one out of six data points had a failure strain less than 2.0%. These failure strains suggest that the energy deposition limits for FeCrAl would be similar to those proposed in DG-1327 for unirradiated fuel [5]. The failure limit parametrized as a function of burnup could look very different as the mechanical properties of FeCrAl evolve.

It is notable that the PCMI limit is not the only relevant cladding performance limit during RIA for FeCrAl cladding. The cladding may also fail during the high temperature phase caused by a boiling crisis (e.g. departure from nucleate boiling in a PWR). There are observed differences in measured critical heat flux with FeCrAl cladding [14-16], but these phenomena are outside the scope of the present article. Nevertheless, they would influence the potential energy deposition limits for FeCrAl cladding in LWRs.

Microstructural analyses are recommended to gain further understanding of the fracture mechanisms. Additional testing without the internal Inconel driver tube is recommended for future work to determine if strain-rate dependence of Inconel impacted the tube specimen's strain-rate dependence. Furthermore, future work will involve developing a technique that is relevant to RIA

performance and can more easily be performed in a hot cell so irradiated material can be tested. The separate effects tests performed in this work directly inform the development of potential integral tests of FeCrAl at the TREAT reactor. Information about bonding between FeCrAl and UO_2 at high burnup, which would influence pellet cladding contact and the loading path during the PCMI phase of RIA, will potentially be provided by post irradiation examination of ongoing irradiation experiments with fueled FeCrAl cladding.

5. Acknowledgments

This research was sponsored by the US Department of Energy Office of Nuclear Energy Advanced Fuels Campaign.

Dr. Nathan Capps and Dr. Aaron Wysocki are acknowledged for their excellent internal review comments on the manuscript.

All authors contributed significantly to this manuscript and the PC MBT effort at ORNL over the past five years. N. R. Brown prepared the draft of the manuscript, helped design the original experimental facility, helped develop the analysis methodology for the current dataset, and provided the relevance to postulated RIA. B. E. Garrison conducted the experiments, analyzed the data, and provided input to the manuscript. R. R. Lowden set up the PC MBT fixtures and assisted in conducting the experiments. M. N. Cinbiz helped design the original experimental facility, developed the DIC instrumentation system, planned the test matrix for these tests, and provided input to the manuscript. K. D. Linton provided the management and coordination for execution of the overall project and provided input to the manuscript.

6. References

[1] Le Coq, A.G., R.C. Martin, and K. Linton, Transportation Planning for Irradiated Fuel-Clad and Integral FeCrAl Experiments, *ORNL/TM-2019/1123*, 2019, Oak Ridge National Laboratory (ORNL), Oak Ridge, TN (United States).

[2] Rebak, R.B., Iron-chrome-aluminum alloy cladding for increasing safety in nuclear power plants. *EPJ Nucl. Sci. Technol.* 3 (2017) 34.

[3] Brown, N.R., A.J. Wysocki, K.A. Terrani, K.G. Xu, and D.M. Wachs, The potential impact of enhanced accident tolerant cladding materials on reactivity initiated accidents in light water reactors. *Ann. Nucl. Energy* 99 (2017) 353–365.

[4] Ott, K.O. and Neuhold, R.J., 1985. *Introductory nuclear reactor dynamics*. American Nuclear Society.

[5] U.S. Nuclear Regulatory Commission, DG-1327, "Pressurized Water Reactor Control Rod Ejection and Boiling Water Reactor Control Rod Drop Accidents", Nov. 2016, (ADAMS Accession No. ML16124A200)

[6] Desquines, J., Koss, D.A., Motta, A.T., Cazalis, B., Petit, M., The issue of stress state during mechanical tests to assess cladding performance during a reactivity-initiated accident (RIA). *Journal of Nuclear Materials,* 412 (2011) 250-267.

[7] Yueh, K., Karlsson, J., Stjärnsäter, J., Schrire, D., Ledergerber, G., Munoz-Reja, C. and Hallstadius, L., 2016. Fuel cladding behavior under rapid loading conditions. *Journal of Nuclear Materials*, *469*, pp.177-186.

[8] Yueh, K., 2017. Applicability of modified burst test data to reactivity initiated accident. *Journal of Nuclear Materials*, *488*, pp.338-345.
[9] Cinbiz, M.N., Brown, N.R., Terrani, K.A., Lowden, R.R. and Erdman III, D., 2017. A pulse-controlled modified-burst test instrument for accident-tolerant fuel cladding. *Annals of Nuclear Energy*, *109*, pp.396-404.
[10] Link, T.M., Koss, D.A. and Motta, A.T., 1998. Failure of Zircaloy cladding under transverse plane-strain deformation. *Nuclear Engineering and Design*, *186*(3), pp.379-394.
[11] Cinbiz, M.N., Gussev, M., Linton, K. and Terrani, K.A., 2019. An advanced experimental design for modified burst testing of nuclear fuel cladding materials during transient loading. *Annals of Nuclear Energy*, *127*, pp.30-38.
[12] Cinbiz, M.N., Koyanagi, T., Singh, G., Katoh, Y., Terrani, K.A. and Brown, N.R., 2019. Failure behavior of SiC/SiC composite tubes under strain rates similar to the pellet-cladding mechanical interaction phase of reactivity-initiated accidents. *Journal of Nuclear Materials*, *514*, pp.66-73.
[13] M. N. Cinbiz, N. R. Brown, R. R. Lowden, M. Gussev, K. Linton, K. A. Terrani. *Report on Design and Failure Limits of SiC/SiC and FeCrAl ATF Cladding Concepts under RIA*, July 2018, ORNL/LTR-2018/521.
[14] Ali, A.F., Gorton, J.P., Brown, N.R., Terrani, K.A., Jensen, C.B., Lee, Y. and Blandford, E.D., 2018. Surface wettability and pool boiling critical heat flux of accident tolerant fuel cladding-FeCrAl alloys. *Nuclear engineering and design*, *338*, pp.218-231.
[15] Lee, S.K., Liu, M., Brown, N.R., Terrani, K.A., Blandford, E.D., Ban, H., Jensen, C.B. and Lee, Y., 2019. Comparison of steady and transient flow boiling critical heat flux for FeCrAl accident tolerant fuel cladding alloy, Zircaloy, and Inconel. *International Journal of Heat and Mass Transfer*, *132*, pp.643-654.
[16] Gorton, J.P., Lee, S.K., Lee, Y. and Brown, N.R., 2019. Comparison of experimental and simulated critical heat flux tests with various cladding alloys: Sensitivity of iron-chromium-aluminum (FeCrAl) to heat transfer coefficients and material properties. *Nuclear Engineering and Design*, *353*, p.110295.

No conflict of interest (N. R. Brown)

N. R. Brown- Conceptualization, Software, Formal analysis, Writing - Original Draft, Supervision, Funding acquisition. B. E. Garrison- Software, Formal analysis, Investigation, Data Curation, Writing - Review & Editing, Visualization. R. R. Lowden- Investigation. M. N. Cinbiz- Conceptualization, Methodology, Investigation, Writing - Review & Editing, Supervision. K. D. Linton- Supervision, Project administration, Funding acquisition.